blood advances®

Development and characterization of prototypes for in vitro and in vivo mouse models of ibrutinib-resistant CLL

Burcu Aslan,[1] Gorkem Kismali,[1] Lisa S. Chen,[1] LaKesla R. Iles,[1] Mikhila Mahendra,[2] Michael Peoples,[2] Mihai Gagea,[3] Natalie W. Fowlkes,[3] Xiaofeng Zheng,[4] Jing Wang,[4] Christopher P. Vellano,[2] Joseph R. Marszalek,[2] Maria Teresa Sabrina Bertilaccio,[1] and Varsha Gandhi[1,5]

[1]Department of Experimental Therapeutics, [2]TRACTION Platform, Therapeutics Discovery Division, [3]Department of Veterinary Medicine and Surgery, [4]Department of Bioinformatics and Computational Biology, and [5]Department of Leukemia, The University of Texas MD Anderson Cancer Center, Houston, TX

Key Points

- We generated cell lines that overexpress wild-type or mutant BTK (BTK^{C481S} and BTK^{C481R}) and mimic ibrutinib-sensitive and -resistant CLL.

- We developed xenograft mouse models by transplanting these cells into Rag2$^{-/-}$ γ$_c$$^{-/-}$ mice to characterize in vivo disease.

Although ibrutinib improves the overall survival of patients with chronic lymphocytic leukemia (CLL), some patients still develop resistance, most commonly through point mutations affecting cysteine residue 481 (C481) in Bruton's tyrosine kinase (BTK^{C481S} and BTK^{C481R}). To enhance our understanding of the biological impact of these mutations, we established cell lines that overexpress wild-type or mutant BTK in in vitro and in vivo models that mimic ibrutinib-sensitive and -resistant CLL. MEC-1 cell lines stably overexpressing wild-type or mutant BTK were generated. All cell lines coexpressed GFP, were CD19$^+$ and CD23$^+$, and overexpressed BTK. Overexpression of wild-type or mutant BTK resulted in increased signaling, as evidenced by the induction of p-BTK, p-PLCγ2, and p-extracellular signal–related kinase (ERK) levels, the latter further augmented upon IgM stimulation. In all cell lines, cell cycle profiles and levels of BTK expression were similar, but the RNA sequencing and reverse-phase protein array results revealed that the molecular transcript and protein profiles were distinct. To mimic aggressive CLL, we created xenograft mouse models by transplanting the generated cell lines into Rag2$^{-/-}$γ$_c$$^{-/-}$ mice. Spleens, livers, bone marrow, and peripheral blood were collected. All mice developed CLL-like disease with systemic involvement (engraftment efficiency, 100%). We observed splenomegaly, accumulation of leukemic cells in the spleen and liver, and macroscopically evident necrosis. CD19$^+$ cells accumulated in the spleen, bone marrow, and peripheral blood. The overall survival duration was slightly lower in mice expressing mutant BTK. Our cell lines and murine models mimicking ibrutinib-resistant CLL will serve as powerful tools to test reversible BTK inhibitors and novel, non–BTK-targeted therapeutics.

Introduction

The B-cell receptor (BCR) pathway is responsible for proliferation, maintenance, and survival of normal and malignant B cells,[1] including those in chronic lymphocytic leukemia (CLL). A pivotal enzyme in the BCR axis is Bruton's tyrosine kinase (BTK),[2] which signals to phospholipase C-γ2 (PLCγ2) and multiple signaling cascades, leading to changes in cell metabolism, transcription, and translation.[3-5] The importance of the BCR pathway, the pathophysiology of CLL, and the prominence of BTK in the BCR signalosome suggest that BTK may be a good therapeutic target.

Ibrutinib binds covalently to the cysteine 481 (C481) residue of the kinase and irreversibly inactivates BTK.[6] Inactivation of BTK results in inhibition of proliferation and dissociates B cells from microenvironmental signals in the lymph nodes, leading to their migration to the peripheral blood.[7]

Preclinical studies using primary CLL cells and TCL-1 mouse models have suggested that ibrutinib is efficacious in several B-cell malignancies.[5,8,9] In the clinic, ibrutinib resulted in impressive overall and progression-free survival with very low untoward toxicity. Thus, the US Food and Drug Administration approved ibrutinib for the treatment of patients with previously treated CLL[10] and for elderly patients with CLL,[11] disease with poor prognosis (eg, those with 17p deletions),[12] and treatment-naive patients.[13]

Although at the early stage, a small percentage of patients develop CLL that is resistant to ibrutinib,[14] the number steadily increases as the length of follow-up increases. Some patients have Richter's transformation, whereas many show CLL progression. Several studies have identified mutations in 2 enzymes in the BCR pathway in prerelapse and postrelapse disease during progression of CLL in patients receiving ibrutinib therapy. These include *BTK* and its immediate downstream kinase, *PLCG2*.[15-18] Of these mutations, the most common are point mutations in the C481 binding site in BTK. Such mutations prevent irreversible drug binding on the C481 site, conferring ibrutinib resistance. For the BTK C481 residue, the site of ibrutinib binding, cysteine-to-serine (C481S) and cysteine-to-arginine (C481R) mutations are the most prevalent.[14] These same mutations are expected to occur with the use of second-generation BTK inhibitors, such as acalabrutinib and zanubrutinib.[19-21]

These data underscore the need to better understand the biology of BTK-mutated CLL and develop new agents that are effective against BTK C481 mutations. However, it is challenging to understand the biology of BTK C481 mutations, because there are currently no models for both in vitro and in vivo use that mimic C481-mutation–related, ibrutinib-resistant CLL. Such a model has been created for MYD88-mutated Waldenström macroglobulinemia and activated B-cell–type diffuse large B-cell lymphoma cells.[22] In CLL, a patient-derived xenograft model has been tested.[23]

In the current study, we developed ibrutinib-resistant CLL cell lines harboring BTK C481S and C481R mutations, compared the biology of these mutant cell lines to that of cell lines with wild-type (WT) BTK, and developed and characterized mouse models with WT and mutant BTK cell lines. Those models could be extended to other B-cell diseases treated with ibrutinib, such as mantle cell lymphoma and Waldenström macroglobulinemia.

Materials and methods

Cell lines and cell cultures

We selected the MEC-1 cell line for this study because it was established using the peripheral blood of a patient with B-cell CLL in prolymphocytoid transformation, and a reproducible xenograft murine CLL model had been developed using this cell line.[24,25] A chromosome analysis of this cell line has been published.[24] Details of the generation of cell lines are provided in the supplemental Methods. All cell lines were routinely screened for *Mycoplasma* species using a MycoAlert *Mycoplasma* Detection Kit (Lonza). Parent

cell lines were authenticated by the Cytogenetics and Cell Authentication Core Facility at MD Anderson Cancer Center.

RNA-sequencing assay

Total RNA was isolated from cells by using an RNeasy Mini Kit (Qiagen) according to the manufacturer's instructions. Samples were sequenced by the Sequencing and Noncoding RNA Program at MD Anderson Cancer Center. Details are provided in the supplemental Methods.

Reverse-phase protein array assay

Exponentially growing MEC-1 cells were seeded (1×10^7 per group) and incubated for 24 hours. The cells were lysed with $1\times$ lysis buffer, and the cellular proteins were denatured in 1% sodium dodecyl sulfate containing β-mercaptoethanol. Lysates were serially diluted and printed on nitrocellulose-coated plates (Grace Bio-Labs) at the Functional Proteomics Reverse Phase Protein Array (RPPA) Core Facility at MD Anderson. Details are provided in the supplemental Methods.

In vivo experiments

We used modified MEC-1 cells to establish a xenograft mouse model.[25] Mice were randomly assigned to 4 groups: no disease (n = 8), BTK^WT^ (n = 10), BTK^C481S^ (n = 10), and BTK^C481R^ (n = 10). Specifically, 1×10^7 MEC-1 cells (BTK^WT^, BTK^C481S^, and BTK^C481R^) were injected IV into 8-week-old female Rag2$^{-/-}\gamma_c^{-/-}$ mice that were monitored daily for development of leukemia and progression. Individual mice were euthanized when they became moribund. At this point, the spleen, liver, left femur, and peripheral blood samples were collected. Cells were isolated and stained with a monoclonal antibody against human CD19-phycoerythrin (PE) clone J3119 (Beckman Coulter), and flow cytometry analysis was performed.

The Institutional Animal Care and Use Committee approved and supervised all animal studies. The mice were cared for in accordance with the guidelines set forth by the American Association for Accreditation of Laboratory Animal Care and the Guide for the Care and Use of Laboratory Animals issued by the US Public Health Service.

Statistical analysis

Unless specified otherwise, all data are expressed as the mean ± SD of results from at least 3 independent experiments. Two-sided Student t tests were used to test the relationships between group means. Survival analysis, Student t tests, and analyses of variance were calculated with GraphPad Prism software. P-values indicate the probability that the difference in the means was due to chance. Other statistical analyses were performed in R software. $P < .05$ denoted statistically significant results.

Results

In vitro characterization of WT and mutant-BTK–expressing cells

We transduced MEC-1 cells to generate cell lines that stably overexpressed GFP, BTK^WT^, and the 2 BTK variants BTK^C481S^ and BTK^C481R^. Overexpression of WT or mutant BTK resulted in increased signaling, as evidenced by levels of induced p-BTK, p-PLCγ2, and phospho-extracellular signal-regulated kinase (p-ERK; Figure 1A).
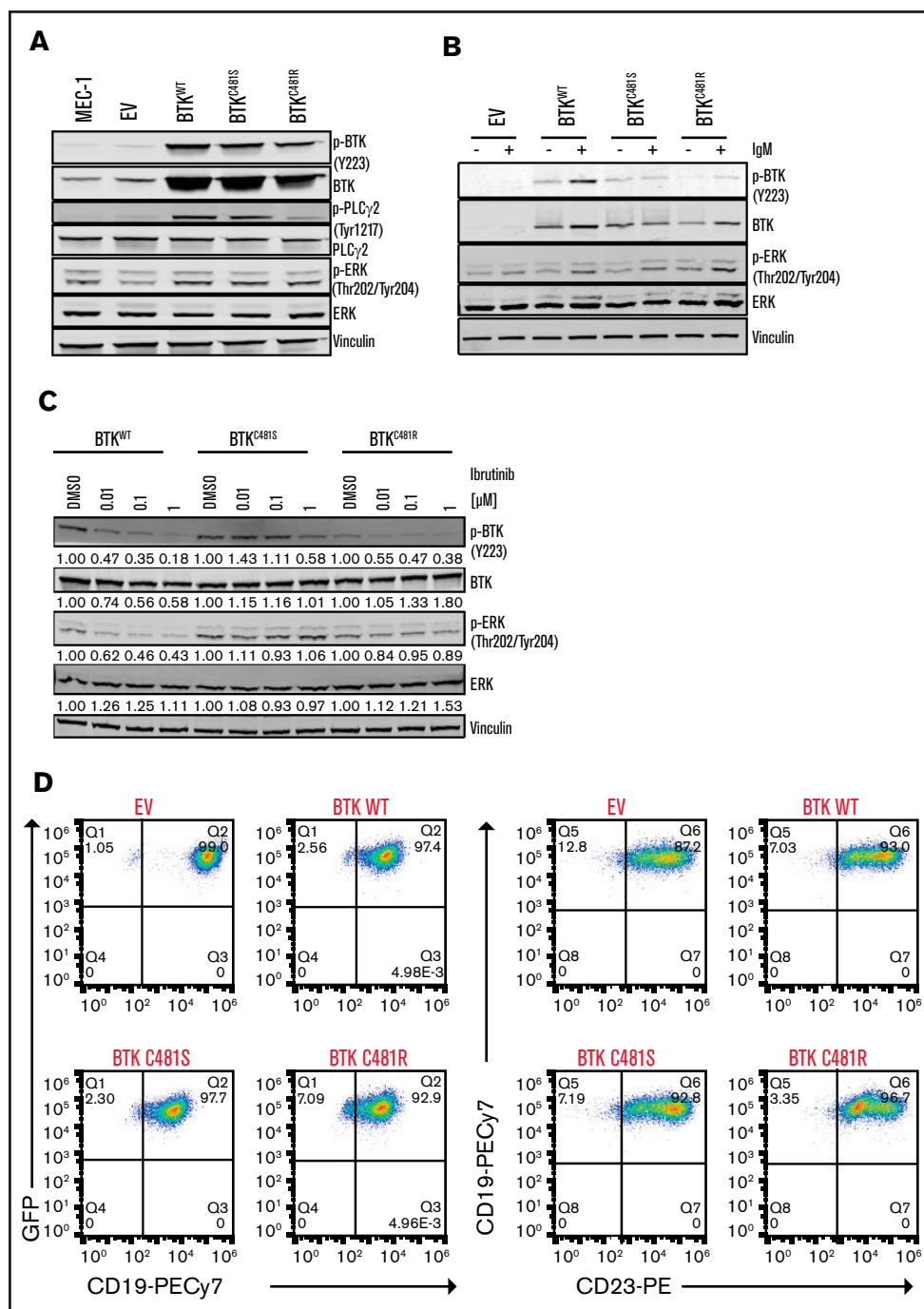
Figure 1. In vitro characterization of MEC-1 cells overexpressing WT and mutant BTK. GFP-labeled MEC-1 cell lines stably overexpressing mutant BTK (BTK^{C481S} or BTK^{C481R}) and BTK^{WT} were generated by using standard lentiviral transduction methods. Cells were sorted to enrich the transduced GFP$^+$ cell populations in each cell line. For all experiments, a population of cells >75% GFP$^+$ was used. (A) Phosphorylated (Y223) and total BTK proteins were overexpressed in transduced cells. p-PLCγ2 (Tyr1217) and p-ERK (Thr202/Tyr204) levels were also increased in all BTK-overexpressing cells. Vinculin was the loading control. (B) IgM stimulation in transduced MEC-1 cells. Cells (5 ×10^5 per milliliter) were seeded in flasks, with or without IgM (20 μg/mL) and incubated at 37°C for 15 minutes. Protein extracts were subjected to immunoblot assays to determine the levels of pBTK (Y223), BTK, pERK (Thr202/Tyr204), and ERK. Vinculin was the loading control. (C) Exponentially growing GFP$^+$ cells were seeded in flasks and incubated with ibrutinib (0.01, 0.1, and 1 μM) for 3 hours. Protein extracts were subjected to immunoblot assays to determine the levels of pBTK (Y223), BTK, pERK (Thr202/Tyr204), and ERK. Vinculin was the loading control. (D) Validation of cell surface markers. Cells were stained with anti-CD19-PECy7 and anti-CD23-PE monoclonal antibodies and analyzed with a flow cytometer. Flow cytometry dot plots showing GFP$^+$ cells (left) and CD19$^+$CD23$^+$ cells (right) after gating on the GFP$^+$ cell population.
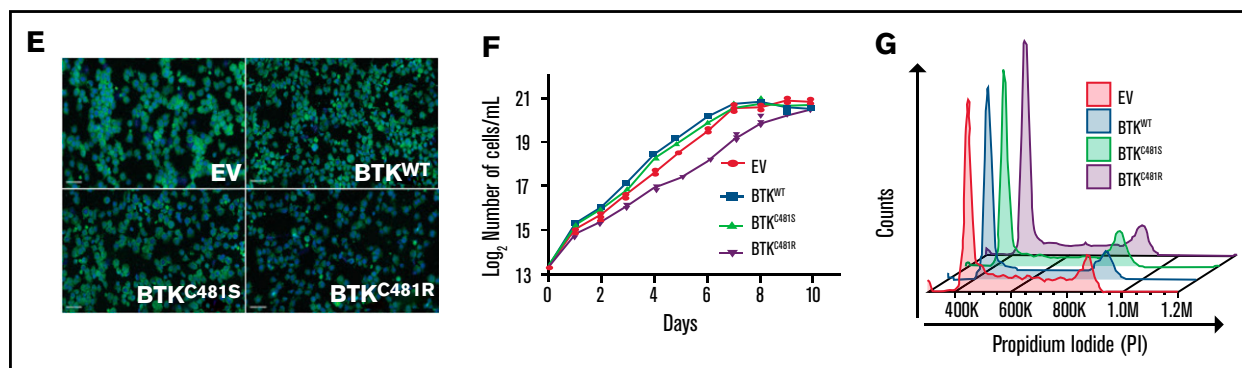
Figure 1. (continued) (E) GFP expression in transduced cell lines. GFP-expressing cells were visualized by fluorescence microscopy, and representative fluorescent photomicrographs were captured and scanned. Original magnification ×40. (F) The growth rates of MEC-1 cells transduced with an EV and MEC-1 cells overexpressing BTK^{WT}, BTK^{C481S}, and BTK^{C481R}. For each cell line, 1×10^5 cells per milliliter were seeded in flasks and counted every day for 10 days with a Coulter counter (n = 3 per group). (G) Cell cycle analyses of each cell line (n = 3 per group). Exponentially growing cells were fixed in 70% ethanol, stained with propidium iodide, and analyzed with flow cytometry. Data are from a representative experiment.

Phospho- and total-BTK levels increased in cells that overexpressed BTK^{WT} and BTK^{C481R}, whereas p-ERK levels increased in all BTK-overexpressing cells upon IgM stimulation (Figure 1B). Ibrutinib treatment dramatically decreased the p-BTK and pERK levels in BTK^{WT} cells. In BTK^{C481S}, pBTK levels did not change at lower concentrations (0.01 and 0.1 μM); however, the levels decreased at the highest concentration (1 μM). In addition, pERK levels did not change in BTK^{C481S} and slightly decreased (10% to 15% inhibition) in BTK^{C481R} upon incubation with ibrutinib for 3 hours (Figure 1C).

CLL is defined as the expansion of monoclonal, mature CD5$^+$CD23$^+$ B cells in the peripheral blood, secondary lymphoid tissues, and bone marrow,[26] and CLL cells typically coexpress CD19, CD5, and CD23. We determined that >90% of the cells in each of our cell lines showed GFP, CD19, and CD23 positivity (Figure 1D). Because all transduced cell lines coexpressed GFP, we were able to enrich the transfected population by using flow cytometry to sort GFP$^+$ cells. Representative images captured by fluorescence microscopy also confirmed that GFP was expressed in all of the generated cell lines (Figure 1E).

The growth rates of the MEC-1 cell lines with WT and mutant BTK were similar; however, cells harboring BTK^{C481R} showed slower proliferation rates, which was significantly different from the empty vector (EV), BTK^{WT}, and BTK^{C481S} cell lines (Figure 1F). Furthermore, we did not observe any distinct distributions of populations in cell cycle profiles, and the differences between group means among the cell lines were not statistically significant (Figure 1G). The percentages of cells in each cell cycle phase are presented in supplemental Table 2. Overall, these data demonstrate that all generated cell lines are CD19$^+$ and CD23$^+$, coexpress GFP, overexpress BTK, and have active BCR signaling and similar cell cycle profiles.

Transcriptomic profiling of WT and mutant-BTK-expressing cells

To identify potential molecular subtypes and associated pathway features in these cell lines, we performed RNA sequencing (RNAseq)–based transcriptomic profiling. The differentially expressed genes (DEGs) showed significant (greater than twofold) changes in transcriptional expression ($q < .05$). Principal component analysis showed a clear separation between BTK^{EV} cells and the cell lines overexpressing BTK (BTK^{WT}, BTK^{C481S}, and BTK^{C481R}; supplemental Figure 1). Overexpression of WT BTK led to 166 upregulated and 69 downregulated DEGs in BTK^{WT} cells, compared with BTK^{EV} cells (supplemental Figure 2A). The comparison of all BTK-overexpressing cell lines with BTK^{EV} revealed 80 upregulated and 15 downregulated DEGs in common (supplemental Figure 2B-C). The overexpression of WT BTK (BTK^{WT} vs BTK^{EV}) led to DEGs that were involved in various signaling pathways, such as those for axonal guidance, G-protein–coupled receptor, ephrin receptor, cyclic adenosine 5′-monophosphate–mediated, paxillin, and CXCR4 signaling (supplemental Figure 3A). Among the DEGs identified, there were 19 transcription factors (*AFF3*, *ETS1*, *FHL5*, *FOXO3*, *GLIS3*, *HLX*, *ID1*, *KLF9*, *KLF11*, *LEF1*, *LMO4*, *NFATC1*, *SIX4*, *TBX15*, *VDR*, *ZEB2*, *ZPF30*, *ZNF114*, and *ZNF532*). The top 3 canonical pathways that were associated with these transcription factors were the epithelial-mesenchymal–transition pathway (*ETS1*, *LEF1*, and *ZEB2*), senescence pathway (*ETS1*, *FOXO3*, *NFATC1*), and interleukin-7 (IL-7) signaling pathway (*FOXO3*, *NFATC1*). In addition, there were 11 transmembrane receptors, 13 transporter proteins, 9 G-protein–coupled receptors, and 7 cytokines altered in BTK^{WT} compared with BTK^{EV} cells.

Next, we compared BTK^{WT} cells with mutant-BTK–expressing cells, as these 3 cell lines overexpress BTK. There were 22 upregulated and 23 downregulated transcripts in BTK^{C481S} cells compared with BTK^{WT} cells (Figure 2A-B). In contrast, the comparison of BTK^{WT} and BTK^{C481R} cells identified only 8 upregulated and 7 downregulated transcripts, indicating the similarity of these 2 cell lines at the transcriptomic level (Figure 2C-D). There were 2 DEGs (*FYB* and *PKIB*) that were upregulated and 3 (*COL5A3*, *ABCC12*, and *NBEA*) that were downregulated in both BTK^{C481S} and BTK^{C481R} cells compared with BTK^{WT} cells. A comparison of the 2 resistant variants (BTK^{C481S} vs BTK^{C481R}) showed 46 upregulated and 20 downregulated DEGs (Figure 2E-F). The top canonical pathways that were identified in
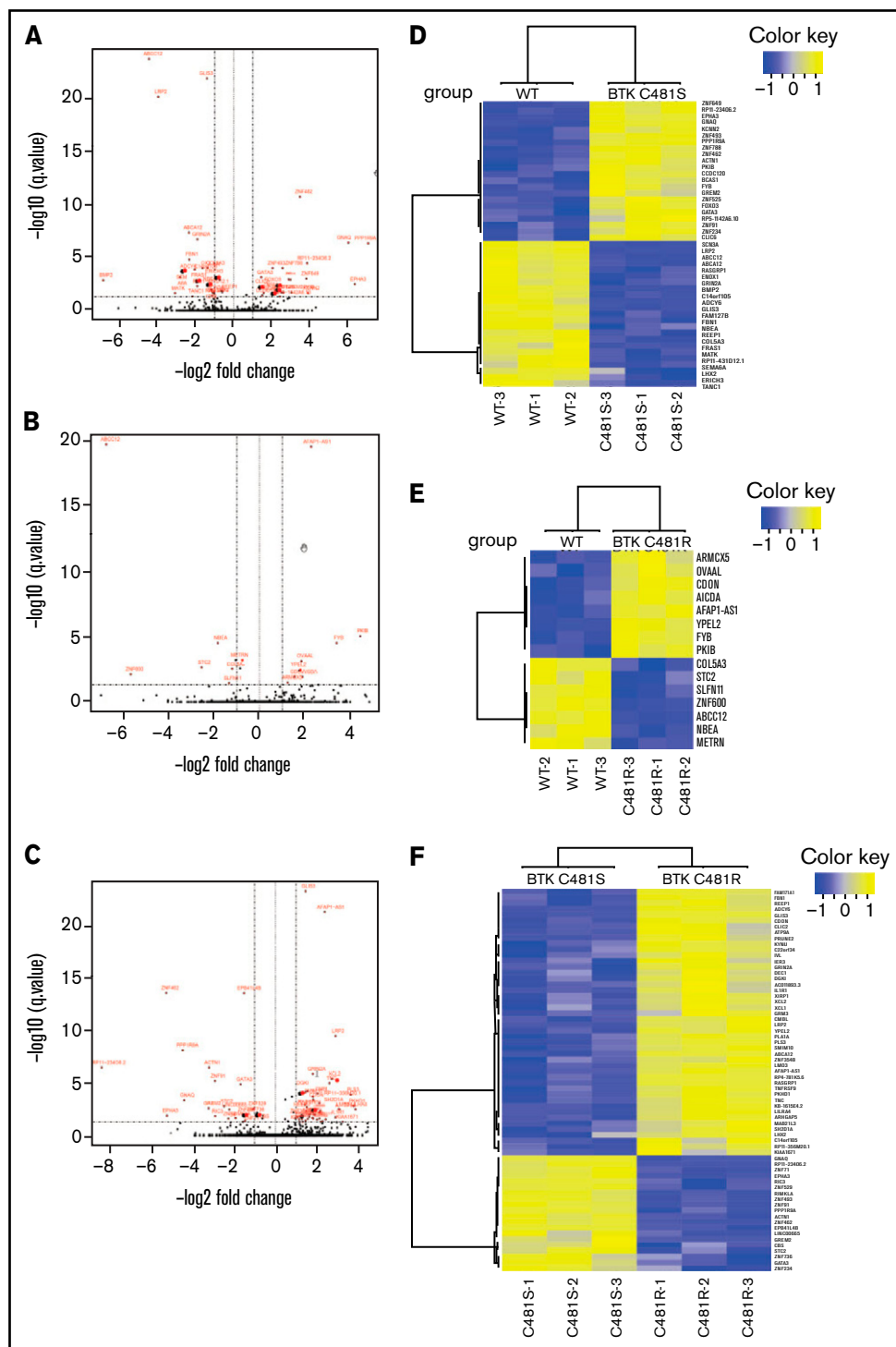
Figure 2. Comparison of the transcriptomic profiles of WT and mutant-BTK–overexpressing cells. (A-C) Volcano plots comparing MEC-1 cells overexpressing BTK^{WT} and BTK^{C481S} (A), BTK^{WT} and BTK^{C481R} (B), and BTK^{C481S} and BTK^{C481R} (C). The DEGs (FDR, ≤0.05; fold change, >2 or < −2) are labeled in red. (D-F) Heat maps of the DEGs (FDR, ≤0.05; fold change, >2 or < −2) between MEC-1 cells overexpressing BTK^{WT} and BTK^{C481S} (D), BTK^{WT} and BTK^{C481R} (E), or BTK^{C481S} and BTK^{C481R} (F).

these comparisons are provided in supplemental Figure 3. These data demonstrate that all of the generated cell lines presented distinct molecular profiles at the transcript level; however the BTK overexpression rather than BTK mutations had a profound effect on the MEC-1 cell biology.

Functional protein profiling for WT and mutant-BTK–overexpressing MEC-1 cells

We first compared RPPA data (426 proteins) in all BTK-overexpressing cell lines (BTK^{WT}, BTK^{C481S}, and BTK^{C481R}) to data

from the BTK^{EV} cell line. Fold changes of the linear expression values were used to generate the representative heat map in Figure 3A (cutoff fold changes, >1.2 or <0.8). The canonical pathways associated with each comparison are provided in supplemental Figure 4.

Seven proteins (COL6A1, FOXO3, HES1, PAR, PDCD1, STAT3, and RPS6_pS240/244) showed changes in all 3 cell lines (BTK^{WT}, BTK^{C481S}, and BTK^{C481R}) relative to the BTK^{EV} cell line (Figure 3B). Among these targets, we were able to validate PDCD1 (PD-1) and Gab2 (Figure 3C). In addition, our immunoblot results showed that p-Pyk2 (Y402), Lyn, and glycogen synthase levels were higher in all BTK-overexpressing cell lines than in parental MEC-1 cells and BTK^{EV} cells.

Next, we compared the BTK-overexpressing cell lines. The top 10 canonical pathways associated with these comparisons were identified with Ingenuity Pathway Analysis and analyzed using the log2 ratios (Figure 3D). The comparison of the BTK^{WT} and BTK^{C481S} cells identified the top 3 canonical pathways as those for IL-15 production (IGF1R, INSR, PTK2, and Syk), BCR signaling (Gab2, PTK2, PTK2B, PTPRC, and Syk), and ERK/MAPK signaling (DUSP4, EIF4EBP1, PAK1, PTK2, and PTK2B). The top 10 canonical pathways in BTK^{WT} relative to BTK^{C481R} cells include chemokine signaling (MAPK14, PRKCA, PTK2, and PTK2B), BCR signaling (Gab2, MAPK14, PTK2, and PTK2B) and ERK/MAPK signaling (DUSP4, PRKCA, PTK2, and PTK2B). When we compared the 2 cell lines expressing the variants BTK^{C481S} and BTK^{C481R}, the top 3 canonical pathways were those for CD28 signaling in T-helper cells (CSK, PAK1, PIK3CA, CD45, and Syk), PI3K/AKT signaling (FOXO3, Gab2, GYS1, MCL1, and PIK3CA), and IL-3 signaling (Gab2, PAK1, PIK3CA, and PRKCA).

To integrate protein and messenger RNA (mRNA) data, we compared those 2 parameters and identified 7 targets (SMAD1, FOXO3, CCNE1, INSR, HES1, CD38, and PHGDH) that were significantly correlated in all of the cell lines compared (supplemental Figure 5). Taken together, these data demonstrate that all of the generated cell lines presented distinct molecular profiles at the transcript and protein levels.

Establishment of and tumor development in xenograft mouse models harboring BTK^{WT}, as well as BTK^{C481S} and BTK^{C481R} mutants

For the in vivo studies, we used transduced MEC-1 cell lines to establish a xenograft mouse model engrafted into Rag2$^{-/-}\gamma_c^{-/-}$ mice. This model mimics aggressive CLL.[25] After injection with one of the transduced MEC-1 cell lines, mice were monitored daily for development and progression of leukemia. We detected a loss of body weight in all groups ∼2 weeks after cell inoculation. After a month, all mice had developed CLL-like disease with systemic involvement (engraftment efficiency, 100%). Individual mice were euthanized when they became moribund and on the advice of our Veterinary Medicine Core service. At this time, the body weight, spleen, liver, peripheral blood and left femur of each mouse were collected. There were no statistically significant differences in body weight among the groups (Figure 4A). We observed splenomegaly, an increased number of localizations in the spleens and livers (macroscopic image shown later in Figure 7), and macroscopically evident areas of necrosis. BTK^{C481R} group had the lowest spleen/body weight ratio, but there were no statistically significant

differences in liver weights ($P < .05$; Figure 4B-C). The duration of overall survival was slightly shorter in mice that were injected with MEC-1 cells harboring mutant BTK (log-rank test; $P = .0001$; Figure 4D).

Localization of GFP$^+$ WT and mutant-BTK–expressing cells in mice

Flow cytometric studies confirmed leukemic expansion of CD19$^+$ GFP$^+$ cells in the spleen (Figure 5A), bone marrow (Figure 5B), and peripheral blood (data not shown). Because we had observed that GFP$^+$ cells could lose GFP expression in vitro over time, we assessed the levels of CD19$^+$ cells in the spleen and bone marrow samples to identify the leukemic B-cell populations. We found substantial accumulations of CD19$^+$ cells in the spleens of all of the mice (Figure 5C); there were no significant differences among the 3 subtypes. However, in the bone marrow analysis, the percentage of mutant BTK cells was greater than that of the BTK^{WT} cells; the greatest localization in all groups was of BTK^{C481S} cells (Figure 5D). Infiltration of MEC-1 cells was observed in the spleen, liver, and bone (Figure 6) of all groups overexpressing BTK. Data from the morphologic diagnosis of organs and a summary of the mean scores for each evaluation are provided in supplemental Table 3.

Histopathology of lymphoid and nonlymphoid tissues in the xenograft system

Compared with the mice in the no-disease group, the remaining 3 groups showed similar spleen sizes at the end point of the study (Figure 7). Fluorescence microscopy showed that there were extensive accumulations of GFP$^+$ MEC-1 cells in the spleens of the mice from the 3 BTK-overexpressing groups, and a higher number of nodules was also observed in those mice (supplemental Figure 6A-B). The cells from the spleens of all groups showed homogenous immunoreactivity for both human CD19 and human CD20, indicating the presence of transplanted MEC-1 cells, given that Rag2$^{-/-}\gamma_c^{-/-}$ mice lack B cells. In addition, all evaluated spleens contained Ki67$^+$ cells, suggesting high MEC-1 cell proliferation rates in all groups.

In contrast to the splenic tissues, the liver tissues in all groups showed localized expression of CD19$^+$ and CD20$^+$ MEC-1 cells (Figure 7). Likewise, these cells were equally proliferative, as indicated by their degree of Ki67 positivity. Similar observations were made in the bone marrow (Figure 7). To assess Ki67 positivity quantitatively, all of the liver slides were scanned with a digital scanner. The livers from all groups, except the no-disease group, showed ∼70% Ki67 positivity. There was no statistically significant difference among the groups overexpressing WT or mutant BTK (supplemental Figure 7). In addition, the splenic and liver tissues (n = 3 per group) were stained with p-S6 antibody, and the staining intensity was quantified. The intensity of p-S6 was slightly higher in the splenic tissues from the groups with mutant BTK than in the BTK^{WT} group (supplemental Figure 8A), whereas it was similar in the liver tissues from all groups (supplemental Figure 8B).

Discussion

Point mutations in BTK at C481 prevent drug binding, which leads to ibrutinib-resistant clones. The absence of in vitro and in vivo models harboring these clones has left unanswered questions about the
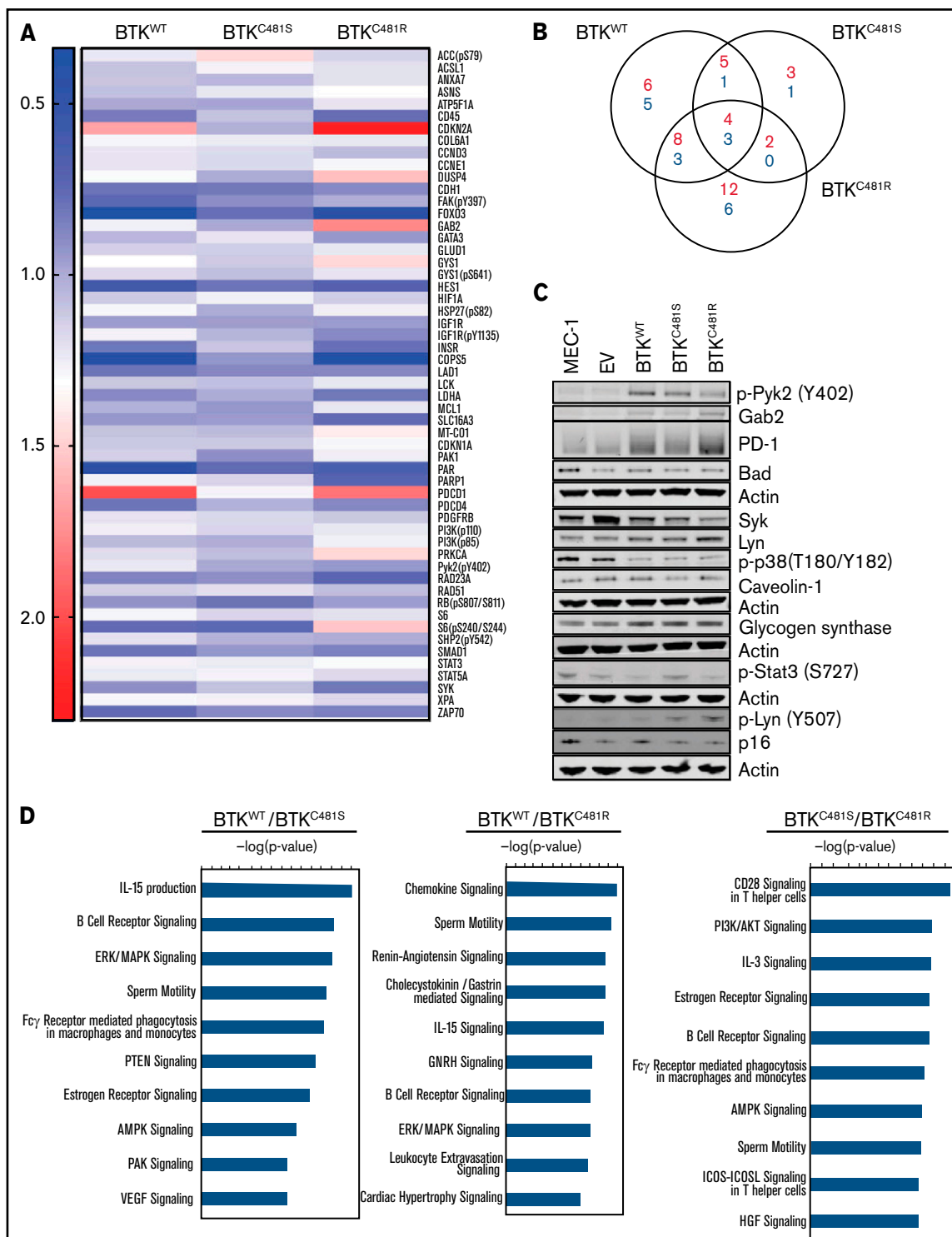
Figure 3. Functional protein profiling of WT and mutant-BTK–overexpressing MEC-1 cells. Protein was extracted in biological triplicates from exponentially growing MEC-1 cells with either WT or mutant BTK and subjected to RPPA assays that included 426 antibodies. (A) Representative heat map of proteins with increased and decreased expression in each cell line (n = 3 per cell line). All BTK-overexpressing cell lines (BTK[WT], BTK[C481S], and BTK[C481R]) were compared with the BTK[EV] cell line. The fold changes of mean linear values were used to generate the heat map (fold change, ≥1.2 or ≤0.8). The color key indicates the fold change. (B) The number of increased (red) and decreased (blue) phosphorylated and total proteins in each transduced cell line compared with the cell line with the empty vector. (C) Validation of RPPA data for some proteins by immunoblot analysis. Protein extracts were subjected to immunoblot assays. To cover all of these proteins, 5 separate immunoblots were prepared, with actin used as the loading control for each. (D) The top 10 canonical pathways identified with Ingenuity Pathway Analysis and associated with the indicated BTKs.
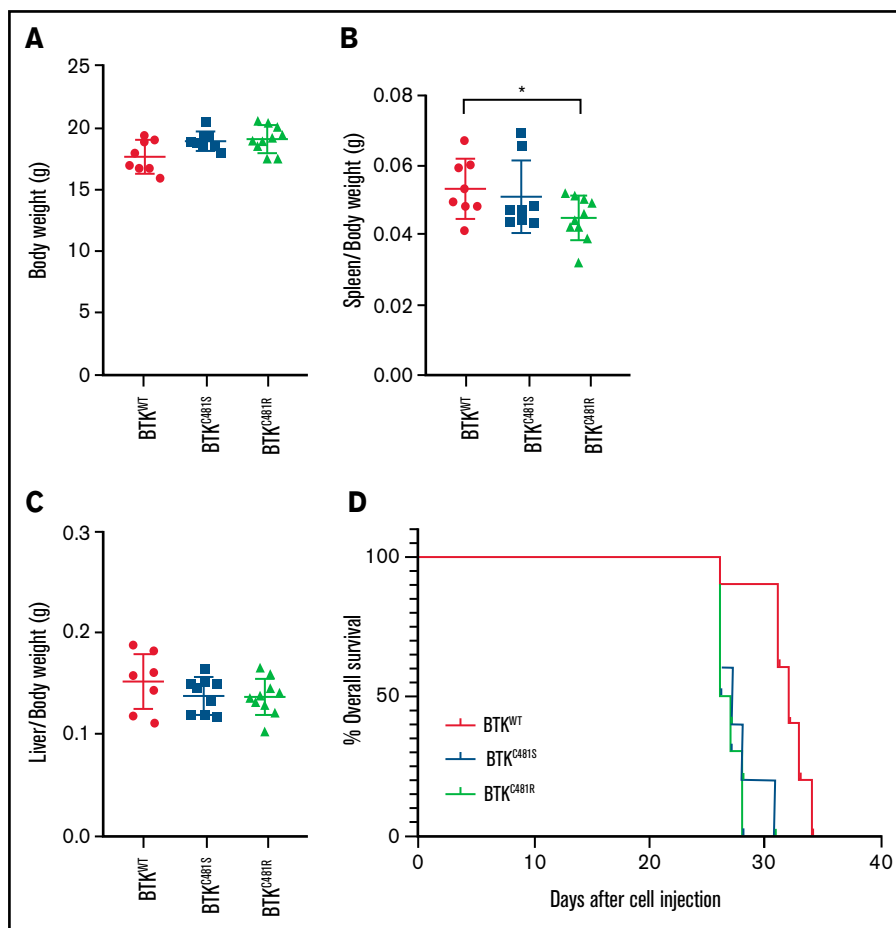
Figure 4. Comparison of in vivo parameters and tumor development in WT and mutant-BTK–expressing MEC-1 cells. MEC-1 cells harboring WT or mutant BTK were injected into 8-week-old $Rag2^{-/-}\gamma_c^{-/-}$ female mice (n = 10 per group), and the animals were monitored for body weight and development and progression of leukemia. At the end point of the study, the spleens, livers, and femurs were collected and macroscopically evaluated. (A) Body weight of mice (n = 10 per group) in each cohort. (B) Spleen/body weight ratios of mice in each cohort (n = 8 BTK[WT], n = 9 BTK[C481S], n = 10 BTK[C481R]; *P < .05). (C) Liver/body weight ratios of mice in each cohort (n = 8 BTK[WT], n = 9 BTK[C481S], n = 10 BTK[C481R]). Groups were compared by fitting a linear mixed-effect model for analysis of variance. (D) Kaplan-Meier curves depict the overall survival of mice in each group (n = 10 per group; mutant vs WT, log-rank test; P = .0001).

biology of ibrutinib resistance and patients' responses to new agents that are effective against these resistant clones. Accordingly, in this study, we established in vitro and in vivo CLL models that harbor either overexpressed WT BTK or BTK point mutations (C481S or C481R) that mimic those observed in patients with ibrutinib-resistant CLL.

The impact of BTK mutation on leukemic cell proliferation was not previously known. In our study, several indicators suggested that the rate of proliferation did not differ in cells harboring either mutant or WT BTK. The growth rate and doubling time of these cells were similar in culture, although BTK[C481R] cells grew slightly more slowly. The cell cycle profiles were comparable. The proliferative index, determined by the level of the Ki67^{+} cell count, further demonstrated that, in the liver, the in vivo proliferation of all 4 BTK subtypes was similar. Collectively, these data suggest that overexpression of WT BTK or mutant BTK[C481S/C481R] does not result in the increased proliferation of cells.

Mouse models are powerful tools for investigating the biology of and therapeutic responses to novel agents. The most remarkable

characteristic of CLL murine models is the penetrance of the CLL phenotype. $E\mu$-TCL1 was the first transgenic mouse model of CLL-like disease,[27,28] and it has the highest penetrance (~100%) of all murine CLL models[29] and has been used to test numerous novel therapeutic strategies.[30] In a recent study, researchers generated a double-transgenic mouse model ($E\mu$-TCL1xMyc) to study therapeutic strategies in concurrent CLL and B-cell lymphoma.[31] However, the $E\mu$-TCL1 model typically requires 6 months for the appearance of circulating tumor cells.[29] In contrast, xenotransplantation of MEC-1 cells provides a more immediate preclinical tool. Our mouse model developed disease in 1 month with 100% engraftment efficiency, which would allow for the efficacy of inhibitors to be determined in a 30-day period. Further, the use of engineered MEC-1 cell lines enabled us to have not only an in vivo model that mimics ibrutinib-resistant CLL but also isogenic cell lines for in vitro use.

CLL cells in humans reside in the bone marrow, lymph nodes, and peripheral blood,[4] whereas in mice they are primarily in the spleen. The spleen size and density changed dramatically in the diseased compared with the disease-free animals; however, spleen size was
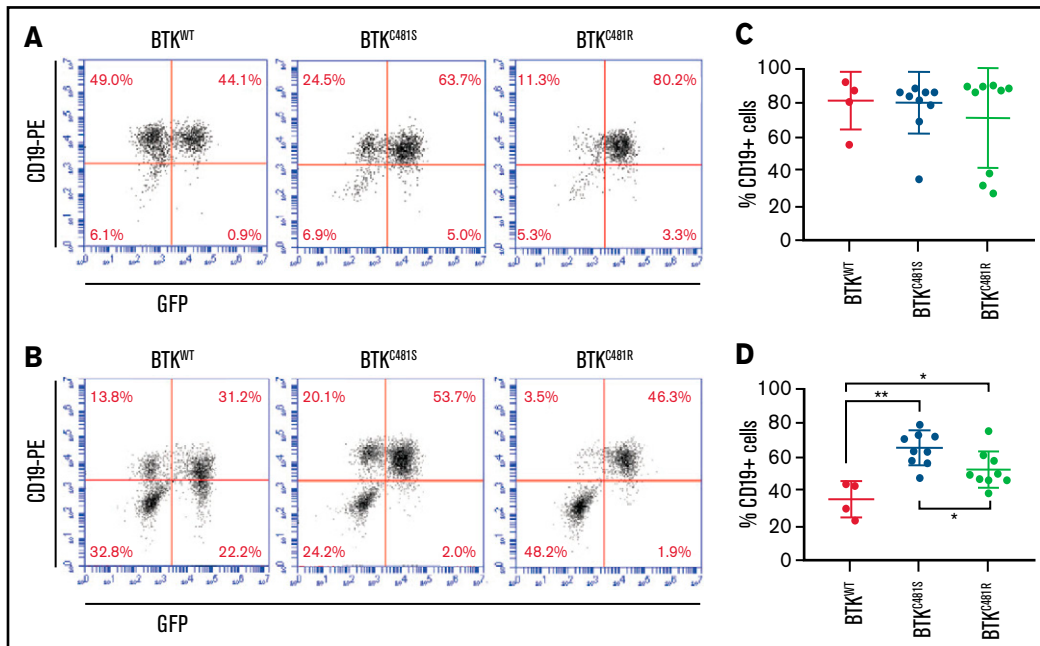
Figure 5. Localization of GFP$^+$ and mutant-BTK–expressing MEC-1 cells in mice. Tumors were established from MEC-1 cells harboring WT or mutant BTK, as described in Figure 4. (A-B) Representative flow cytometry plots for the spleen and bone marrow samples collected from mice with BTK^{WT} (n = 4; left), BTK^{C481S} (n = 9; center), and BTK^{C481R} (n = 9; right). At the time of euthanization, cells were collected from the spleen (A) and bone marrow (B), stained with a monoclonal antibody against human CD19 to identify the GFP$^+$ MEC-1 cells, and analyzed by flow cytometry. (C-D) The percentage of CD19$^+$ MEC-1 cells in spleen (C) and bone marrow (D). One-way analysis of variance, $P = .05$; Student t test, $*P < .05$ for BTK^{WT} vs BTK^{C481R} cells; $**P < .01$ for BTK^{WT} vs BTK^{C481S} cells.

similar among the BTK^{WT}, BTK^{C481R}, and BTK^{C481S} mice. The spleen/body weight ratio in the BTK^{C481R} mice was significantly lower than that in the BTK^{WT} mice; this result may be attributable to the slightly lower proliferation rate of BTK^{C481R} cells compared with BTK^{WT} cells. In the spleens, the number of CD19$^+$ cells per 100 000 cells was similar in all groups, whereas in the bone marrow, there were significantly more CD19$^+$ cells in the mutant groups than in the BTK^{WT} group, and this factor may be
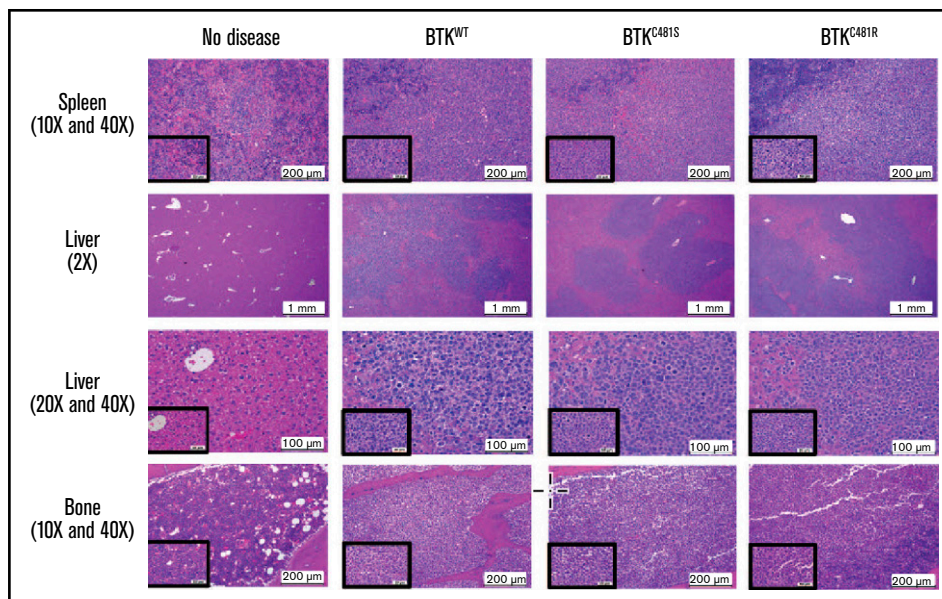
Figure 6. Histopathological assessment of tissues. Histopathologic assessments of hematoxylin and eosin–stained slides were conducted by a veterinary pathologist. Representative images of tissues and lesions of lymphocytic infiltration were captured at the indicated magnifications for the main and inset images. The evaluation results, including the morphologic diagnoses of the organs and the summaries of the mean scores, are provided in supplemental Table 3. Liver and spleen: n = 8/no disease, n = 8/EV, n = 8/BTK^{WT}, n = 9/BTK^{C481S}, and n = 9/BTK^{C481R}. Bone: n = 8/no disease, n = 6/EV, n = 7/BTK^{WT}, n = 6/BTK^{C481S}, and n = 6/BTK^{C481R}.
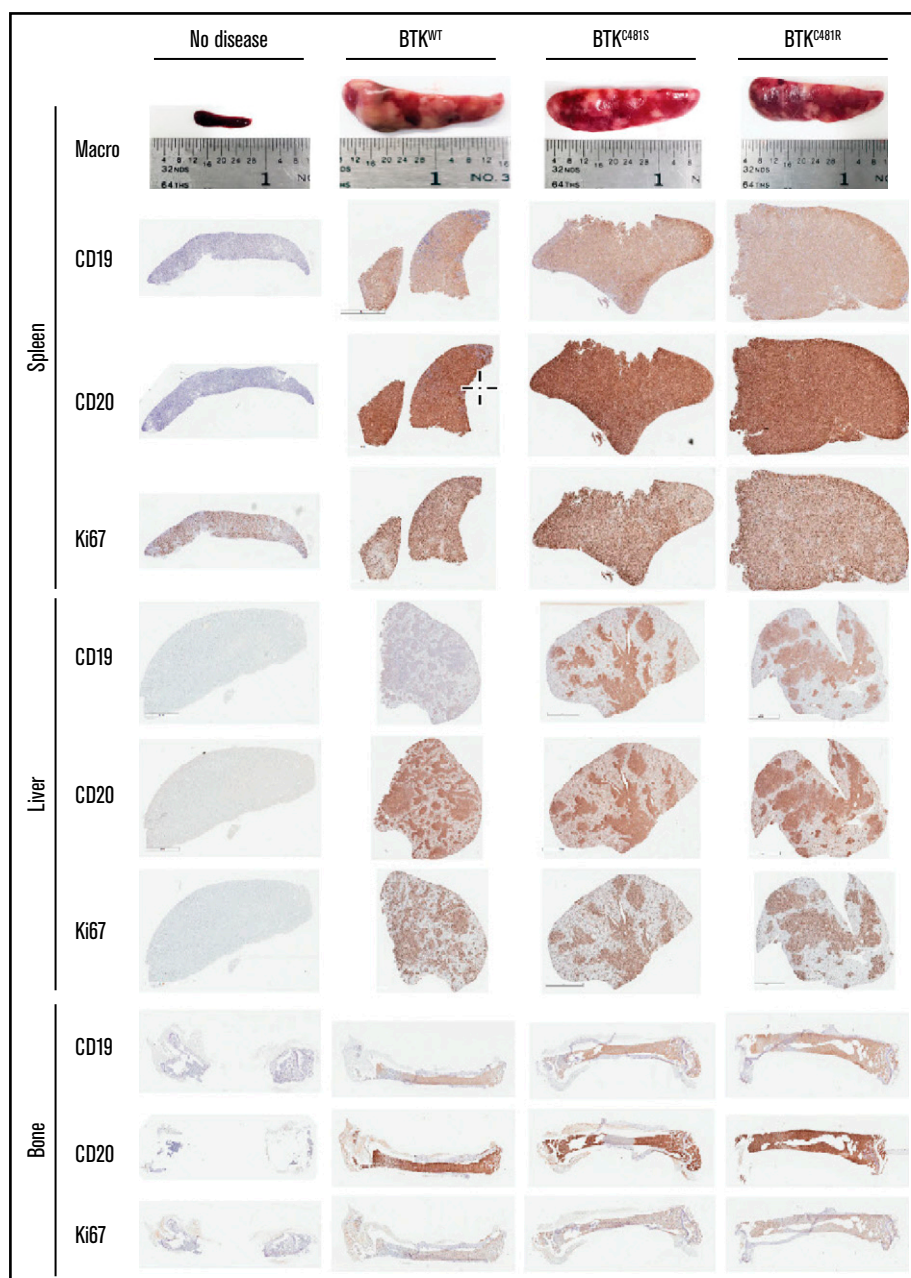
Figure 7. Immunohistochemical analyses of spleen, liver, and bone tissues after the establishment of disease from MEC-1 cells with WT or mutant BTK. Representative macroscopic images of spleens from each group are provided in the top row. Spleen, liver, and bone tissues were collected at the time of euthanasia. B-cell marker expression (CD19 and CD20) and proliferation marker expression (Ki-67) are shown for the spleen, liver, and bone marrow from mice with no disease and from BTK[WT], BTK[C481S], and BTK[C481R] mice.

contributory to the early demise of mice with mutant-BTK–harboring MEC-1 cells. There are 2 possible reasons for increased CD19^{+} cells: either the cells harboring mutant BTK proliferated more in the bone marrow or these cells interacted better with the microenvironment and remained in the bone marrow for a longer time. Our in vitro data on the proliferation rates of the cell lines do not support the first possibility. Thus, further studies are needed to explain the interaction between the BTK mutant cells and the microenvironment in vivo.

A significant benefit of studying the resistant clones in vitro was the ability to explore the molecular signatures associated with overexpression of this enzyme as well as the mutational status of the kinase. First, our focus was on the targets that were altered by BTK overexpression, regardless of BTK mutation status. It was clear from the omics data that mere overexpression of the enzyme resulted in profound changes in DEGs. Some of these changes could be explored further with respect to development of resistance. For instance, Gab2 increased in all BTK-overexpressing cell lines

(BTK^{WT}, BTK^{C481S}, and BTK^{C481R}) compared with BTK^{EV}, per both our RNAseq and RPPA data, and the protein levels were validated by our immunoblot results. Acquired ibrutinib resistance from exposure to escalating doses of the drug resulted in increased BTK and Gab2 expression in the Namalwa B-cell lymphoma cell line.[32] Gab2 expression has also been reported to be significantly higher in the bone marrow of patients with chronic myeloid leukemia than in controls.[33] In addition, Kim and colleagues[34] recently identified Gab2 as a previously unrecognized target that altered DNA methylation in Korean patients with CLL.

Next, we compared mutant-BTK–expressing cells to BTK^{WT} cells. This comparison revealed 5 common DEGs (NBEA, COL5A3, ABCC12, FYB, and PKIB) that were altered in mutant compared with BTK^{WT} cells. We also identified targets that were previously reported to be associated with CLL or other hematologic malignancies. For instance, EphA3, GNAQ, and GATA3 mRNA levels were higher in BTK^{C481S} than in BTK^{WT} cells. Previously, an aberrant EphA3 copy number was found to be associated with multiple types of hematologic malignancies,[35,36] and mRNA levels correlated positively with the copy numbers.[36] Recently, driver mutations in *GNAQ* and *GATA3* have been identified in a patient with CLL.[37-39] We observed that GATA3 transcript and protein levels were higher in BTK^{C481S} than in BTK^{WT} cells; however, the levels in patients with CLL remain unknown, and the clinical outcomes associated with the expression levels of these targets should be studied.

In the integrative analyses of RNAseq and RPPA results, only 7 genes had adjusted $P < .05$ (SMAD1, FOXO3, CCNE1, INSR, HES1, CD38, and PHGDH). It is important to underscore that there are only 426 proteins in this RPPA panel. SMAD1 expression was lower in all BTK-overexpressing cell lines at both the transcript and protein levels. It has been shown that the TGF-β-SMAD pathway is inactivated in CLL[40] and has a role in follicular lymphoma.[41] In addition, SMAD1 expression is aberrantly downregulated in >85% of patients with diffuse large B-cell lymphoma and provides a proliferative advantage to B cells in vitro and in vivo.[42]

Our transcriptomic and proteomic data delineated molecular differences between WT and BTK-mutant MEC-1 cells. Importantly, between the 2 variants (C481S and C481R), we identified differential expression of both proteins and transcripts. Collectively, our data confirm the distinct molecular signatures of these subclones that may lead to context-specific resistance and further the development of personalized medicine and potential combination strategies.

A limitation of our study is the lack of validation of our findings in patients harboring BTK subclones. The primary reason for this is that there are insufficient numbers of purified CLL cells from patients with these mutations. Therefore, further evaluation with clinical data are needed for a comprehensive characterization. Nonetheless, our current work is of value because it established in vitro and in vivo ibrutinib-resistant prototypes harboring the most prominent BTK C481 mutations or overexpression of WT BTK. Because the engraftment, expansion, and dissemination of these BTK cells in lymphoid and nonlymphoid tissues mimics human CLL, our models may be valuable preclinical tools for understanding the pathophysiology of the disease and testing a new generation of reversible BTK inhibitors that do not require C481 binding. These new-generation BTK inhibitors

include Loxo-305,[43,44] vecabrutinib,[45-47] and ARQ 531,[48] which bind to an allosteric site of the kinase and inhibit BTK and its downstream signaling. These agents are in early clinical development for patients with relapsed/refractory CLL and mantle cell lymphoma and are primarily intended for those in whom therapy with irreversible BTK inhibitors has failed. Currently, we are testing a reversible BTK inhibitor in this model system. In addition, our in vitro and in vivo models may provide a tool for evaluating combination strategies that could be tested and validated in cell lines and animals before clinical use. Finally, our modified MEC-1 cell line and xenograft mouse models could be a context-specific model system applicable to other C481 or PLCγ2.

Acknowledgments

Authorship

Contribution: B.A. designed and performed the experiments, analyzed the results, and wrote the first draft of the manuscript; G.K. assisted in all in vivo experiments and in planning the work; L.S.C. and L.R.I. assisted at the end point of the in vivo experiments; M.M. and M.P. worked on the construction of the plasmids for all of the BTK clones and the establishment of cell lines following transduction; M.G. evaluated all of the pathology results and contributed to the writing of the manuscript; N.W.F. captured images of the cells with a fluorescence microscope; X.Z. performed all of the bioinformatics analyses of the RPPA and RNAseq data; J.W. supervised X.Z.; C.P.V. supervised M.M. and M.P.; J.R.M. supervised M.M. and M.P., participated in intellectual discussions regarding model systems, and wrote and reviewed the manuscript; M.T.S.B. directed the in vivo experiments for the development of the mouse models and wrote and reviewed the manuscript; and V.G. conceptualized and supervised the research, obtained funding, analyzed the data, and wrote and reviewed the manuscript.

Conflict-of-interest disclosure: V.G. has sponsored research agreements from Sunesis and Loxo Oncology. The remaining authors declare no competing financial interests.

The current affiliation for G.K. is Department of Biochemistry, Ankara University Faculty of Veterinary Medicine, Ankara, Turkey.

ORCID profiles: B.A., 0000-0003-1852-9079; V.G., 0000-0002-3172-9166.

Correspondence: Varsha Gandhi, Department of Experimental Therapeutics, The University of Texas MD Anderson Cancer Center, Unit 1950, 1901 East Rd, Houston, TX 77054; e-mail: vgandhi@mdanderson.org.

References

1. Stevenson FK, Krysov S, Davies AJ, Steele AJ, Packham G. B-cell receptor signaling in chronic lymphocytic leukemia. *Blood.* 2011;118(16):4313-4320.

2. Ponader S, Burger JA. Bruton's tyrosine kinase: from X-linked agammaglobulinemia toward targeted therapy for B-cell malignancies. *J Clin Oncol.* 2014;32(17):1830-1839.

3. Bernal A, Pastore RD, Asgary Z, et al. Survival of leukemic B cells promoted by engagement of the antigen receptor. *Blood.* 2001;98(10):3050-3057.

4. Howard DR, Munir T, McParland L, et al. Clinical effectiveness and cost-effectiveness results from the randomised, Phase IIB trial in previously untreated patients with chronic lymphocytic leukaemia to compare fludarabine, cyclophosphamide and rituximab with fludarabine, cyclophospha-mide, mitoxantrone and low-dose rituximab: the attenuated dose rituximab with chemotherapy in chronic lymphocytic leukaemia (ARCTIC) trial. *Health Technol Assess.* 2017;21(28):1-374.

5. Herman SE, Mustafa RZ, Gyamfi JA, et al. Ibrutinib inhibits BCR and NF-κB signaling and reduces tumor proliferation in tissue-resident cells of patients with CLL. *Blood.* 2014;123(21):3286-3295.

6. Honigberg LA, Smith AM, Sirisawad M, et al. The Bruton tyrosine kinase inhibitor PCI-32765 blocks B-cell activation and is efficacious in models of autoimmune disease and B-cell malignancy. *Proc Natl Acad Sci USA.* 2010;107(29):13075-13080.

7. Spaargaren M, Beuling EA, Rurup ML, et al. The B cell antigen receptor controls integrin activity through Btk and PLCgamma2. *J Exp Med.* 2003;198(10):1539-1550.

8. Herman SE, Gordon AL, Hertlein E, et al. Bruton tyrosine kinase represents a promising therapeutic target for treatment of chronic lymphocytic leukemia and is effectively targeted by PCI-32765. *Blood.* 2011;117(23):6287-6296.

9. Ponader S, Chen S-S, Buggy JJ, et al. The Bruton tyrosine kinase inhibitor PCI-32765 thwarts chronic lymphocytic leukemia cell survival and tissue homing in vitro and in vivo. *Blood.* 2012;119(5):1182-1189.

10. Byrd JC, Brown JR, O'Brien S, et al; RESONATE Investigators. Ibrutinib versus ofatumumab in previously treated chronic lymphoid leukemia. *N Engl J Med.* 2014;371(3):213-223.

11. O'Brien S, Furman RR, Coutre SE, et al. Ibrutinib as initial therapy for elderly patients with chronic lymphocytic leukaemia or small lymphocytic lymphoma: an open-label, multicentre, phase 1b/2 trial. *Lancet Oncol.* 2014;15(1):48-58.

12. O'Brien S, Jones JA, Coutre SE, et al. Ibrutinib for patients with relapsed or refractory chronic lymphocytic leukaemia with 17p deletion (RESONATE-17): a phase 2, open-label, multicentre study. *Lancet Oncol.* 2016;17(10):1409-1418.

13. Burger JA, Tedeschi A, Barr PM, et al; RESONATE-2 Investigators. Ibrutinib as initial therapy for patients with chronic lymphocytic leukaemia. *N Engl J Med.* 2015;373(25):2425-2437.

14. Woyach JA, Furman RR, Liu T-M, et al. Resistance mechanisms for the Bruton's tyrosine kinase inhibitor ibrutinib. *N Engl J Med.* 2014;370(24):2286-2294.

15. Woyach JA, Ruppert AS, Guinn D, et al. BTKC481S-mediated resistance to ibrutinib in chronic lymphocytic leukemia. *J Clin Oncol.* 2017;35(13):1437-1443.

16. Burger JA, Landau DA, Taylor-Weiner A, et al. Clonal evolution in patients with chronic lymphocytic leukaemia developing resistance to BTK inhibition. *Nat Commun.* 2016;7(1):11589.

17. Ahn IE, Underbayev C, Albitar A, et al. Clonal evolution leading to ibrutinib resistance in chronic lymphocytic leukemia. *Blood.* 2017;129(11):1469-1479.

18. Silvia Bonfiglio LS, Gaidano G, Trentin L, et al. Half of chronic lymphocytic leukemia patients relapsing under ibrutinib carry btk and plcg2 mutations: a European Research Initiative on CLL (Eric) real-world study [abstract]. Presented at the Annual Meeting of the European Hematology Association. 17 June 2018. Abstract LB2601.

19. Patel V, Balakrishnan K, Bibikova E, et al. Comparison of acalabrutinib, a selective Bruton tyrosine kinase inhibitor, with ibrutinib in chronic lymphocytic leukemia cells. *Clin Cancer Res.* 2017;23(14):3734-3743.

20. Byrd JC, Harrington B, O'Brien S, et al. Acalabrutinib (ACP-196) in relapsed chronic lymphocytic leukemia. *N Engl J Med.* 2016;374(4):323-332.

21. Tam CS, Quach H, Nicol A, et al. BGB-3111 in combination with obinutuzumab in patients with chronic lymphocytic leukemia and follicular lymphoma [abstract]. *Blood.* 2017;130(suppl 1). Abstract 1745.

22. Chen JG, Liu X, Munshi M, et al. BTK^{Cys481Ser} drives ibrutinib resistance via ERK1/2 and protects BTK$^{wild-type}$ MYD88-mutated cells by a paracrine mechanism. *Blood.* 2018;131(18):2047-2059.

23. Robinson HR, Qi J, Cook EM, et al. A CD19/CD3 bispecific antibody for effective immunotherapy of chronic lymphocytic leukemia in the ibrutinib era. *Blood.* 2018;132(5):521-532.

24. Stacchini A, Aragno M, Vallario A, et al. MEC1 and MEC2: two new cell lines derived from B-chronic lymphocytic leukaemia in prolymphocytoid transformation. *Leuk Res.* 1999;23(2):127-136.

25. Bertilaccio MTS, Scielzo C, Simonetti G, et al. A novel Rag2⁻/⁻gammac⁻/⁻-xenograft model of human CLL. *Blood.* 2010;115(8):1605-1609.

26. Bosch F, Dalla-Favera R. Chronic lymphocytic leukaemia: from genetics to treatment. *Nat Rev Clin Oncol.* 2019;16(11):684-701.

27. Bichi R, Shinton SA, Martin ES, et al. Human chronic lymphocytic leukemia modeled in mouse by targeted TCL1 expression. *Proc Natl Acad Sci USA.* 2002;99(10):6955-6960.

28. Johnson AJ, Lucas DM, Muthusamy N, et al. Characterization of the TCL-1 transgenic mouse as a preclinical drug development tool for human chronic lymphocytic leukemia. *Blood.* 2006;108(4):1334-1338.

29. Simonetti G, Bertilaccio MTS, Ghia P, Klein U. Mouse models in the study of chronic lymphocytic leukemia pathogenesis and therapy. *Blood.* 2014;124(7):1010-1019.

30. Bresin A, D'Abundo L, Narducci M, et al. TCL1 transgenic mouse model as a tool for the study of therapeutic targets and microenvironment in human B-cell chronic lymphocytic leukemia. *Cell Death Dis.* 2016;7(1):e2071.

31. Lucas F, Rogers KA, Harrington BK, et al. Eμ-TCL1xMyc: A Novel Mouse Model for Concurrent CLL and B-Cell Lymphoma. *Clin Cancer Res.* 2019;25(20):6260-6273.

32. Farag SM, Newton D, Doody G, et al. Molecular mechanisms of ibrutinib resistance: defining a logical approach to improving targeted therapy in CLL [abstract].*Blood.* 2016;128(22). Abstract 2046

33. Aumann K, Lassmann S, Schöpflin A, et al. The immunohistochemical staining pattern of Gab2 correlates with distinct stages of chronic myeloid leukemia. *Hum Pathol.* 2011;42(5):719-726.

34. Kim M, Lee E, Zang DY, et al. Novel genes exhibiting DNA methylation alterations in Korean patients with chronic lymphocytic leukaemia: a methyl-CpG-binding domain sequencing study. *Sci Rep.* 2020;10(1):1085.

35. Keane N, Freeman C, Swords R, Giles FJ. EPHA3 as a novel therapeutic target in the hematological malignancies. *Expert Rev Hematol.* 2012;5(3):325-340.

36. Guan M, Liu L, Zhao X, et al. Copy number variations of EphA3 are associated with multiple types of hematologic malignancies. *Clin Lymphoma Myeloma Leuk.* 2011;11(1):50-53.

37. Hernández-Sánchez M, Kotaskova J, Rodríguez AE, et al. CLL cells cumulate genetic aberrations prior to the first therapy even in outwardly inactive disease phase. *Leukemia.* 2019;33(2):518-558.

38. Puente XS, Beà S, Valdés-Mas R, et al. Non-coding recurrent mutations in chronic lymphocytic leukaemia. *Nature.* 2015;526(7574):519-524.

39. Landau DA, Tausch E, Taylor-Weiner AN, et al. Mutations driving CLL and their evolution in progression and relapse. *Nature.* 2015;526(7574):525-530.

40. Matveeva A, Kovalevska L, Kholodnyuk I, Ivanivskaya T, Kashuba E. The TGF-beta - SMAD pathway is inactivated in cronic lymphocytic leukemia cells. *Exp Oncol.* 2017;39(4):286-290.

41. Munoz O, Fend F, de Beaumont R, Husson H, Astier A, Freedman AS. TGFbeta-mediated activation of Smad1 in B-cell non-Hodgkin's lymphoma and effect on cell proliferation. *Leukemia.* 2004;18(12):2015-2025.

42. Stelling A, Hashwah H, Bertram K, Manz MG, Tzankov A, Müller A. The tumor suppressive TGF-β/SMAD1/S1PR2 signaling axis is recurrently inactivated in diffuse large B-cell lymphoma. *Blood.* 2018;131(20):2235-2246.

43. Mato AR, Shah NN, Jurczak W, et al. Pirtobrutinib in relapsed or refractory B-cell malignancies (BRUIN): a phase 1/2 study. *Lancet.* 2021;397(10277):892-901.

44. Gomez EB, Isabel L, Rosendahal MS, Rothenberg SM, Andrews SW, Brandhuber BJ. Loxo-305, a highly selective and non-covalent next generation BTK inhibitor, inhibits diverse BTK C481 substitution mutations [abstract]. *Blood.* 2019;134(suppl 1). Abstract 4644.

45. Allan JN, Patel K, Mato AR, et al. Ongoing results of a phase 1B/2 dose-escalation and cohort-expansion study of the selective, noncovalent, reversible Bruton's tyrosine kinase inhibitor, vecabrutinib [abstract]. *Blood.* 2019;134;(suppl 1). Abstract 3041.

46. Aslan B, Hubner SE, Fox JA, et al. Vecabrutinib inhibits B-cell receptor signal transduction in chronic lymphocytic leukemia cell types with wild-type or mutant Bruton's tyrosine kinase. *Haematologica.* In press.

47. Fabian CA, Reiff SD, Guinn D, et al. SNS-062 demonstrates efficacy in chronic lymphocytic leukemia in vitro and inhibits C481S mutated Bruton tyrosine kinase [abstract]. *Cancer Res.* 2017;77(13 suppl). Abstract 1207.

48. Reiff SD, Mantel R, Smith LL, et al. The BTK inhibitor ARQ 531 targets ibrutinib-resistant CLL and Richter transformation. *Cancer Discov.* 2018;8(10):1300-1315.